Compact fiber-optic vector inclinometer

Li-Yang Shao[1,2,*] and Jacques Albert[1]

[1]*Department of Electronics, Carleton University, 1125 Colonel By Drive, Ottawa, Ontario, Canada K1S 5B6*
[2]*Institute of Optoelectronic Technology, China Jiliang University, Hangzhou 310018, China*
*Corresponding author: liyangshao@gmail.com

What we believe to be a novel fiber-optical inclinometer based on a dual-path core-to-cladding mode coupling mechanism is demonstrated. Both the amplitude and tilt direction of bends about a 2-mm-long flexure joint in an optical fiber can be determined. The sensor head consists of a nonadiabatic abrupt taper cascaded with a weakly tilted fiber Bragg grating. Measured bend angles of up to 12° are demonstrated, as well as a method to increase the sensitivity for bend angles smaller than 4°. © 2010 Optical Society of America

OCIS codes: 060.2370, 060.3735.

Tilted fiber Bragg grating (TFBG) sensors benefit from a wide range of sensing modalities and they are easy to fabricate: in a TFBG, the grating planes are slightly tilted from the fiber axis, which enhances the coupling of light from the core mode to a large number of counterpropagating cladding modes. The differential sensitivity of core and cladding modes has been employed to construct temperature-independent strain sensors [1] and refractive index sensors [2], for instance. Usually, TFBG sensors require the measurement of the power spectrum of the transmitted light, which may be a problem in some instances where a single-ended sensor would be preferable (*in vivo* applications, for instances). While a standard TFBG can be used in reflection with help from a mirror downstream from the TFBG (a cleaved fiber, coated or not, or another fiber Bragg grating) [2], it is also possible to recouple into the core some of the light propagating backward in the cladding [3–5]. With such recoupling, several peaks appear in the reflection spectrum corresponding to several cladding mode resonances in addition to the core mode back-reflection, and all the TFBG sensing modalities become available in single-ended reflection mode and further allow measurements using bandpass-filtered power levels instead of complete power spectra [3–5]. The best device to use as a core-cladding mode coupler is a nonadiabatic but low loss taper, as it does not require splices between similar or dissimilar fibers and is very easy to fabricate in a fiber at arbitrary small distances from any other device in the fiber, such as a TFBG. We used such a taper in [5] to demonstrate a TFBG accelerometer where a beam containing both the taper and TFBG was subjected to large radius curvatures under dynamic loading. These experiments further showed that the response of this device depends strongly on the direction of the applied curvature (as expected for bent TFBGs [5]), thereby requiring separate knowledge of the direction to measure the magnitude of the vibration.

In the present Letter, and in contrast to the accelerometer structure used in [5], we fix the TFBG in a straight tube and only allow the 2-mm-long taper region to bend. The great advantage of this simple improvement is that for bend angles between 2° and 12° we can determine both the bend angle and its direc-tion using simple bandpass-filtered power measurements: the core mode reflected power depends "only" on the bend magnitude, while the cladding mode reflected power depends on "both" the magnitude and direction of the bend. This contrasts with previous reports where several gratings are needed to determine two parameters simultaneously [6]. Furthermore, by selecting different passbands for the cladding mode power measurement, the sensitivity can be optimized for different ranges of angles. We believe that this device will find many applications in structural health monitoring especially for deformations of large structures that involve angles between 2° and 12° [7].

Fiber tapers have been intensively investigated as power couplers, beam shapers, and sensors [8–10]. Adiabatic tapers have a small taper angle and the coupling between the core mode and the cladding modes is negligible, resulting in low loss devices. But when the taper angle increases, it has been demonstrated that coupling can occur between core and cladding modes [11]. A microscope photo of the taper with a waist diameter of 66.7 μm and a length of $\sim$600 μm is shown in Fig. 1(a). Using these values, we have calculated the normalized frequency number V at the waist of the taper to be 0.95, which is smaller than the "core mode cutoff" number ($V_{cc} \approx 1$), and the maximum local taper angle to be 0.01 rad, well above the nonadiabatic threshold [11].

While a cylindrically symmetric taper can only couple the fundamental core mode to cladding modes of the same azimuthal symmetry, bending the taper greatly enhances the number of modes that can be coupled [12] and also changes the coupling coefficients of different cladding modes according to their field patterns relative to the bend direction. We now proceed to show that while the only measurable parameter of a single-mode taper is power loss, from which only the magnitude of a bend can be estimated as shown in [10] (a combined taper and long period grating structure), adding a noncylindrically symmetric cladding mode recoupling mechanism downstream from the taper provides the necessary information to determine the direction of the bend (i.e., in the plane of bending, there remains a ±180° uncertainty about the bend direction within that plane). Here, a TFBG located at a short distance after the
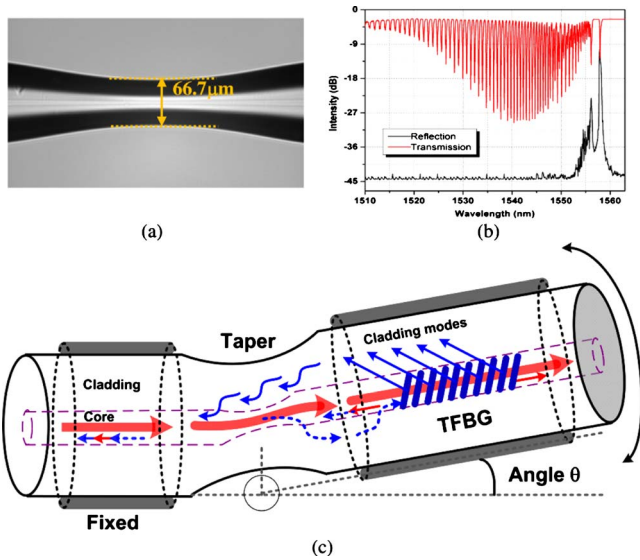
© 2010 Optical Society of America

Fig. 1. (Color online) (a) A microscope photo of the fused taper with a waist diameter of 66.7 μm. (b) Reflection and transmission spectra of a concatenated taper and TFBG. (c) Schematic diagram of the proposed sensor.

taper is introduced to recouple some cladding modes excited at the taper back into the fiber core. The TFBG tilt plane orientation also breaks the cylindrical symmetry and introduces an angular dependence in the recoupling [13]. Therefore we expect that the cladding mode reflected power should depend on the relative orientation of the bend plane of the taper and the tilt plane of the grating (designated as φ). In addition, the internal tilt angle of TFBGs determines the relative amounts of power in Bragg, ghost, and cladding modes [13], which consequently affects the dynamic range of the bend measurement.

To get all the needed modes, a 10-mm-long 5.5° tilted grating was inscribed in hydrogen-loaded Corning SMF-28 fibers using a pulsed KrF excimer laser with phase mask technique. The nonadiabatic taper was fabricated in the same fiber at a distance of 10 mm before the TFBG, by elongating the fiber using the arc discharge of a commercial fusion splicing machine. The fusion parameters are adjustable to control the diameter of the taper waist (discharge current, arc duration, and the tension applied on the fiber). The fabrication parameters for the taper with a waist diameter of 66.7 μm were as follows: current=12.5 mA, arc duration=800 ms, tension =10 g. The resulting taper has a broadband insertion loss of 1.6 dB. Figure 1(b) shows the reflection and transmission spectra of the concatenated taper and TFBG. In addition to the usual Bragg reflection near 1558 nm, we see that several cladding mode resonances appear in the reflection spectrum at shorter wavelengths because of recoupling at the taper (cladding modes from TFBGs alone are never observed in reflection because they are quickly attenuated in fiber patch cords or radiated away at connectors). Finally, Fig. 1(c) shows the schematic diagram of the proposed sensor and the three possible paths that the incident core guide light can take. The first path corresponds to core guided light reflected back in the core at the Bragg wavelength of the grating. Light at

that wavelength is simply attenuated twice by the taper [our gratings have reflectivities greater than 90% for most of the modes involved as can be seen from Fig. 1(b)]. For the second path, core guided light that went through the taper but at shorter wavelengths gets coupled to the backward cladding modes by the TFBG and some of those cladding modes get recoupled to the fiber core by the taper. The total loss for this path includes the core mode transmission through the taper, the magnitude of the core-cladding coupling of the TFBG, and the magnitude of the recoupling from the cladding modes to the core. Finally, the third path shows the core-guided light coupled to some cladding modes by the taper getting recoupled to a backward core mode by the TFBG (while the taper coupling is not wavelength selective, the backward recoupling into the core by the TFBG can occur only at wavelengths shorter than the Bragg wavelength). For this path, the backward-propagating core light is attenuated one more time in going through the taper. For simplicity, we can express the power reflected from the core mode (P_B) and from ith order cladding mode (P_C^i) in the following manner:

$$P_C^i = 2T_t^i(\theta)[1 - T_t^i(\theta)]C^i(\varphi), \qquad (1)$$

$$P_B = [T_t^0(\theta)]^2 R_B^0, \qquad (2)$$

where the input light power is assumed as 1, and θ and φ are the magnitude and direction of bend. $T_t^0(\theta)$ is the transmission of core guided mode and $T_t^i(\theta)$ is the coupling coefficient between the core mode and the ith order cladding mode through the taper. $R_B^{(0)}$ and $C^i(\varphi)$ denote, respectively, the reflectivity of the core mode upon itself and the coupling between the ith order cladding mode and the core in the TFBG (the latter is dependent on the bend direction). The factor of 2 in Eq. (1) arises because of the two paths involving cladding modes that yield the same contribution to P_C^i. For the real sensor corresponding to Fig. 1(c), the fibers before and after the taper are protected by capillary tubes with an inner diameter of 128 μm. The distances from the center of the taper to each of the two capillary tubes are equal to 1 mm. The capillary tube ensures that the TFBG is kept straight at any bend angle θ. In the experiment, one capillary tube was fixed and the other was bent from $-12°$ to $+12°$ around an origin at the center of the taper. Figure 2 depicts the evolution of the full reflection spectra for several bend angles (0°, 4°, 8°, and 12°). The reflection of the core mode (longest wavelength) decreases while that of higher-order cladding modes (shortest wavelengths) increases with the bend angle. The change in the lower order cladding modes (resonance wavelengths closest to the Bragg wavelength) saturates quickly but provides higher sensitivity at small angles. The opposite occurs for higher-order modes. Therefore we can use two different bandpass filters to optimize the sensor's response to different bend angle ranges: 1554.5–1555.5 nm for small angles ($\pm4°$) and 1543–1553 nm for the full range ($\pm12°$). The filter for the core mode reflection remains centered at 1558 nm with a 1 nm bandwidth.
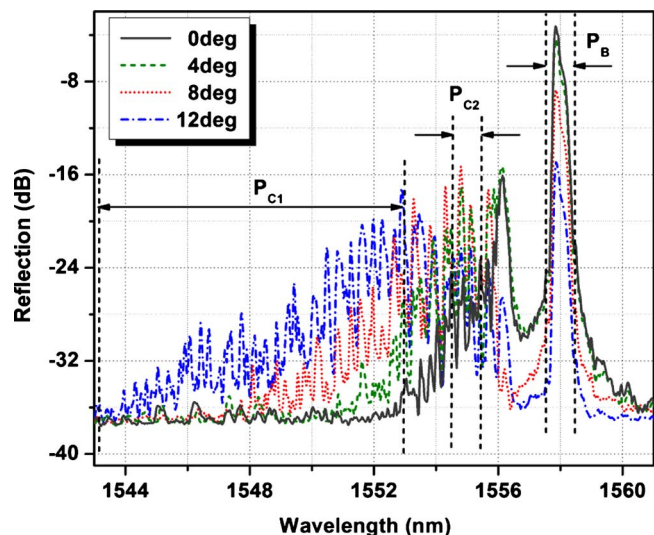
Fig. 2.   (Color online) Reflection spectra evolution against the bend angle.

Using the additional degree of freedom provided by the angle of the tilt plane direction of the TFBG relative to the bend direction, we further determined that the core mode reflection (P_b) is insensitive to this angle, unlike P_c which shows a maximum and a minimum sensitivity for two orthogonal bending directions. The results are shown in Fig. 3, where "Max" and "Min" stand for two orthogonal bending directions (φ) with maximum and minimum sensitivities. We can see that the orientation of the bend yields large differences in the reflected power of the cladding modes but none for the core mode. Figure 3 also shows that by selecting low-order cladding modes with a suitable bandpass filter enhances the bend sensitivity considerably for bend angles smaller than $\pm4°$ (from 0.87 to 2.3 dB/deg). The typical accuracy of
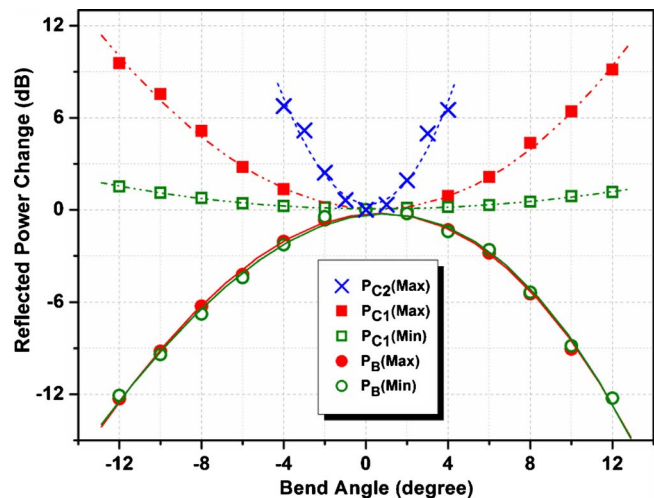

Fig. 3.   (Color online) Reflection power changes against the bend angle for several passbands and bend orientations: P_B is core mode band; P_{C1} is wide cladding mode band; P_{C2} is narrow cladding mode band; Max and Min correspond to the bending orientations that yield maximum and minimum sensitivities.

bend angle measurement, based on comparison of the applied angle to the polynomial fitting value from the experimental data, is $\pm0.15°$. Power normalization of the sensor system can be provided easily by a power tap after the light source because further bend loss for single-mode fibers is negligible in the range of bends considered here.

In summary, we proposed and experimentally demonstrated a concatenated nonadiabatic taper and weakly TFBG to measure the bending angle. While the measurement of bends from the core mode transmission characteristics of nonadiabatic tapers is a well known phenomenon, we have demonstrated that a noncylindrically symmetric cladding–core recoupling mechanism located downstream from the taper further provides information about the direction of the bending by its impact on the device reflection in specific spectral bands. We also demonstrated that the sensitivity of the device can be optimized for different bend angle ranges by selecting the spectral bands over which power measurement is carried out. Since the measurement does not require a high spectral resolution, simple bandpass filters and detectors can be used to keep system costs low. Also as a result of the wide passband used and small temperature sensitivities of the TFBG (10 pm/°C) and taper, the device response will not strongly depend on temperature in typical indoor/outdoor applications. Therefore, we feel that the proposed structure is a potentially interesting candidate lightweight all-fiber solution for measuring bends and inclination of large-scale infrastructures.

References

1. C. Chen and J. Albert, Electron. Lett. **42**, 1027 (2006).
2. C.-F. Chan, C. Chen, A. Jafari, A. Laronche, D. J. Thomson, and J. Albert, Appl. Opt. **46**, 1142 (2007).
3. T. Guo, A. Ivanov, C. Chen, and J. Albert, Opt. Lett. **33**, 1004 (2008).
4. Y. X. Jin, C. C. Chan, X. Y. Dong, and Y. F. Zhang, Opt. Commun. **282**, 3905 (2009).
5. T. Guo, L.-Y. Shao, H.-Y. Tam, P. A. Krug, and J. Albert, Opt. Express **17**, 20651 (2009).
6. H. Bao, X. Dong, C. Zhao, L. Y. Shao, C. C. Chan, and P. Shum, Opt. Commun. **283**, 968 (2010).
7. S. Vurpillot, G. Krueger, D. Benouaich, D. Clément, and D. Inaudi, ACI Struct. J. **95**, 518 (1998).
8. J. D. Love, W. M. Henry, W. J. Stewart, R. J. Black, S. Lacroix, and F. Gonthier, IEE Proc.-J: Optoelectron. **138**, 343 (1991).
9. Y. He and F. G. Shi, Opt. Commun. **260**, 127 (2006).
10. O. Frazão, R. Falate, J. L. Fabris, J. L. Santos, L. A. Ferreira, and F. M. Araújo, Opt. Lett. **31**, 2960 (2006).
11. J. D. Love and W. M. Henry, Electron. Lett. **22**, 912 (1986).
12. L. C. Bobb, P. M. Shankar, and H. D. Krumboltz, J. Lightwave Technol. **8**, 1084 (1990).
13. S. Baek, Y. Jeong, and B. Lee, Appl. Opt. **41**, 631 (2002).